Remarkable 8.3% efficiency and extended electron lifetime towards highly stable semi-transparent iodine-free DSSCs by mitigating the in-situ triiodide generation

Anil Kumar Bharwal, Laura Manceriu, Celine Olivier, Abdelfattah Mahmoud, Cristina Iojoiu, Thierry Toupance, Carmen Ruiz, Marcel Pasquinelli, David Duché, Jean-Jacques Simon, et al.

Remarkable 8.3% efficiency and extended electron lifetime towards highly stable semi-transparent iodine-free DSSCs by mitigating the *in-situ* triiodide generation

Anil Kumar Bharwal [a, b, c *], Laura Manceriu [a *], Celine Olivier [d], Abdelfattah Mahmoud [a], Cristina Iojoiu [b], Thierry Toupance [d], Carmen M. Ruiz [c], Marcel Pasquinelli [c], David Duché [c], Jean-Jacques Simon [c], Catherine Henrist [a], Fannie Alloin [b]

[a] GREENMAT, CESAM Research Unit, University of Liège, Department of Chemistry, Liège 4000, Belgium

[b] Université Grenoble Alpes, Université Savoie Mont Blanc, CNRS, Grenoble INP, LEPMI, Grenoble 38000, France

[c] Aix-Marseille Université, Université de Toulon, IM2NP, UMR 7334 CNRS, Campus de Château-Gombert, Marseille 13453, France

[d] Univ. Bordeaux, CNRS, Bordeaux INP, ISM, UMR 5255, 351 Cours de la Libération, F-33405 Talence, Cédex, France

*Corresponding author: anil.bharwal@im2np.fr;

: laura.manceriu@uliege.be

GRAPHICAL ABSTRACT:

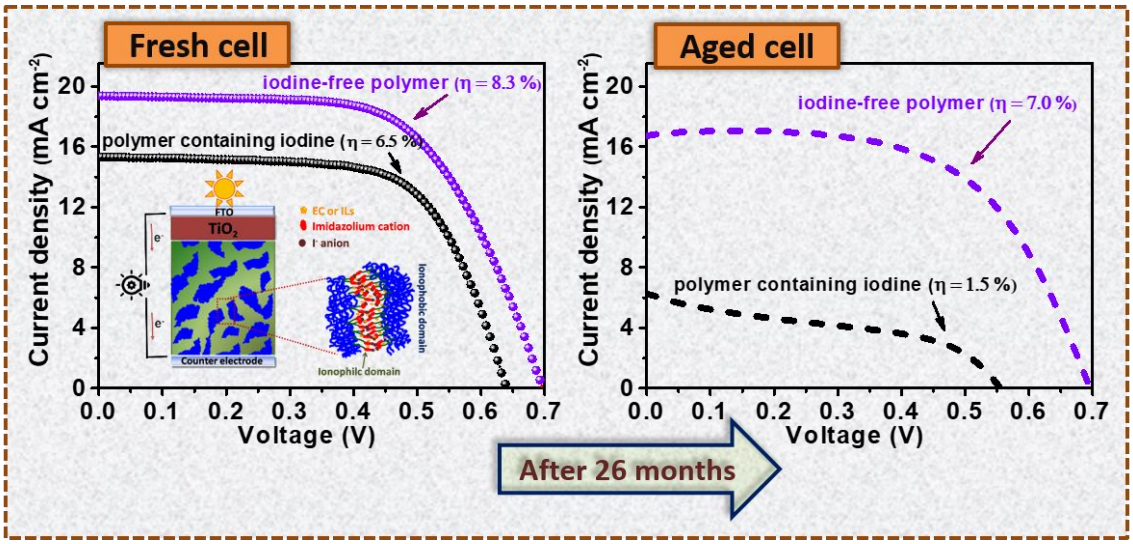

Abstract:

Achieving highly stable and efficient dye-sensitized solar cells (DSSCs) remains a major challenge for future industrial development. In the present work, a series of ionic conductors, such as ionic liquids (ILs), polysiloxane-based poly(ionic liquid)s (PILs), and their blends have been employed as electrolytes in solid-state DSSCs. In particular, we have studied the effect of PILs ionic functionality interaction with the ILs and ethylene carbonate (EC) on the photovoltaic performance of DSSCs with and without I_2. Omitting iodine (I_2) from the electrolytes in fabricated DSSCs enhances both V_{oc} and J_{sc} due to the reduced charge recombination and extended effective electron lifetime. We confirmed through Raman spectroscopy that in I_2-free DSSCs, the *in-situ* generated tri-iodides (I_3^-) ions are sufficient enough to complete the reaction mechanism. Additionally, the I_2-free DSSCs exhibit enhanced transparency, encouraging our efforts towards BPIV suitable applications. When plasticized with EC, the ionic conductivities of the highly functionalized I_2-free PIL-based DSSCs exceeded 10^{-3} S cm^{-1} at 30 ^oC, giving record PCE of 8.3% and 9.1% under standard (1 sun) and modest (0.3 sun) illumination, respectively. These devices also showed excellent long-term stability, retaining about 84% of their initial efficiency after 26 months.

1. Introduction

Since the groundbreaking work by Honda and Fujishima in the 1972s, photoelectrochemical cells gained more and more success and popularity [1]. In 1991, O'Regan and Grätzel reported the fabrication of dye-sensitized solar cells (DSSCs) with the standard I^-/I_3^- liquid electrolyte and a Ru-based dye [2]. In recent years, DSSCs have gained significant attention thanks to their academic and industrial development [3–12]. A typical DSSC is usually made up of three components: a dye coated-TiO_2 electrode that absorbs sun or artificial light, and generates photoexcited electrons, a redox electrolyte for the dye regeneration, and hole transport, and a counter electrode to recover the reduced form of the redox mediator [2,13–15]. In particular, the electrolyte properties impact strongly the device stability and efficiency [16–18]. For a long time, great efforts have been made to achieve efficiencies over 11% for DSSCs fabricated with standard I^-/I_3^- electrolyte [19–21]. A benchmark power conversion efficiency (PCE) of 13% was achieved with new redox couples based on Co-complexes liquid electrolytes associated with porphyrin dye [22–24]. Eventually, the PCE of DSSCs has progressively increased from 7% to 14.3% [2,25,26]. However, practical applications of DSSCs based on these liquid electrolytes are restricted due to solvent leakage and evaporation, not to mention the counter electrode corrosion [27].

To counterbalance those issues, solid-state DSSCs (ss-DSSCs) are fabricated by replacing the liquid electrolytes with inorganic semiconductors, such as CuI, CuSCN, or $CsSnI_{3-x}F_x$ [28–30], or hole-transporting materials, such as P3HT, Spiro-OMeTAD, or amorphous Cu(II/I) [31–33]. However, the efficiency of ss-DSSCs is lower than liquid-state DSSCs due to the surface limited penetration of solid electrolytes into the mesoporous TiO_2 and shortened electron-free path. In recent years, the use of quasi-solid-state electrolytes (QSSEs) based on ionic liquids (ILs) [34,35] and poly(ionic liquid)s (PILs) [36,37] have shown great potential

for preparing quasi-solid state DSSCs. Essentially, PILs as QSSEs are very exciting since they have similar properties to ILs with improved mechanical durability and dimensional control of a polymer [38]. PILs are typically solid or viscous liquids depending on their structure, glass transition temperature (T_g), and molecular weight. Due to these unique properties, PILs are used as electrolytes in DSSCs in various forms e.g. as additives [37,39] or membranes [40–42,36] in liquid electrolytes, in the pure solid form [43,44], as well as in blends with well-matched ILs [43,45,46].

In the last few years, numerous efforts aiming at improving the stability of the DSSCs by using polysiloxane-based electrolytes have been made [47–49]. In our previous work, we systematically studied and investigated the photovoltaic properties of different polysiloxane-based PILs blends with ILs, such as 1-methyl-3 propylimidazolium-iodide (MPII) and 1-methyl-3-propyl-imidazolium-Bis(trifluoromethane)sulfonimide (MPITFSI), and non-ionic liquids such as ethylene carbonate (EC) [46,50,51]. However, all these polymer electrolytes contained iodine (I_2) which affected the durability and limited the performance of the DSSCs due to the I_2 sublimation and incident light absorption, respectively. Furthermore, when present in the electrolyte, I_2 leads to the formation of extra I_3^- that causes photodegradation, counter-electrode corrosion, and dye desorption [52]. The different I_2 concentrations in electrolytes influence the charge transportation and electron recombination dynamics in DSSCs [53]. Ali *et al.* [54] showed that the removal of 50% of I_2 from the QSSCs significantly improved both the stability and the PCE of DSSCs. The first I_2-free DSSC was reported by Wang *et al*. [55] with a PCE of 5.5%, maintaining about 70% of its initial photonic efficiency after one-month storage. Another approaches for fabricating stable solid-state DSSC was the utilization of I_2-free PILs in combination with different hierarchical TiO_2 photoanodes, a combination necessary for avoiding a trade-in of specific surface and electrolyte penetration efficiency. Since then, there have been few attempts to prepare I_2-free DSSCs to improve stability and

PCE. Yu et al. [56] reported DSSCs based on I_2-free liquid electrolytes gelled with 15 wt.% TiO_2 which reached a PCE of 8.0%. Although the PCE value of the resulting I_2-free DSSCs was slightly lower than that of I_2-based DSSCs (8.32%), its long-term at-rest stability was improved. Ahn et al. [57] reported the use of PVC-g-POEM templated, 6 µm thick, mesoporous TiO_2 as photoanode in combination with a solid I_2-free poly((1-(4- ethenylphenyl)methyl)-3-butyl-imidazolium iodide) (PEBII) reaching 7.1 % efficiency. The same authors reported a slightly higher PCE of 7.4 % for honeycomb-like organized, 8.5 µm thick TiO_2 photoanodes in the presence of PEBII [58]. By imbedding double-shell TiO_2 nanosheet-covered SnO_2 hollow spheres in the same templated TiO_2 photoanode the same group managed to improve the dye loading and light-harvesting characteristics reaching 8.2 % efficiency [59]. However, the improved efficiency is more related to the increased light harvesting than to improved electrolyte penetration since there is no evolution in the FF values. Roh et al. [60] reported 8.0% efficiency by using the same solid electrolyte, the PEBII, in combination with a much thicker tree-like nanostructured TiO_2 photoanode. Although the organized TiO_2 photoanodes in these studies ensured a high enough specific surface area for efficient dye-loading and good enough porosity for the solid electrolyte penetration, the opaque design does not facilitate their future building integration.

Thus, new trends in designing transparent DSSCs were developed for maximizing the harvested light and facilitating their building integration. In 2011, Lunt et al. [61] first introduced a fullerene-based organic planar heterojunction transparent photovoltaic technology, showing up to 57% of total transparency and 1.7% PCE. Very recently, Alkarsifi et al. [62] demonstrated the attractive color-tuning properties of organic planar heterojunction based on non-fullerene acceptor ITIC-4F and PBDB-T-2F donor. Henceforth, many efforts have been made in color-tunable and transparent photovoltaic technologies [63–66]. The optical properties of DSSCs can be modified by tuning several parameters such as the dye, the

electrolyte, or the electrodes thicknesses [67–70]. Lately, Chalkias et al. [71] developed a binary approach to fabricating semi-transparent DSSCs by using organic dyes and I_2-free liquid electrolytes. The resulting I_2-free DSSCs exhibited transmittance up to 55%, offering high IPCE (85%) in the whole blue and green part of the visible spectrum.

Recently, we reported improved performance and stability (in both ambient and accelerated aging conditions) of I_2-free DSSCs fabricated with TiO_2 electrodes grown on flexible Ti substrate and polysiloxane ionic conductors as electrolytes [72]. We assumed that the in-situ generation of I_3^- ions in I_2-free DSSCs was sufficient for the DSSC operation. In 2005, Seo et al. [73] presented the first electro-diffuse-reflection spectroscopy study on the I_3^- in-situ generation of I_2-free DSSCs during working conditions. Prehal et al. [74] used in-situ Raman spectroscopy to successfully demonstrate the reversible formation of I_3^-, I_5^-, and I_2 in the carbon nanopores produced by the oxidation of I^-.

In this work, we focused on optimizing the polymer electrolyte composition for a standard randomly-organized TiO_2 photoanode such as to ensure a similar conversion efficiency but enhanced long-term stability of semi-transparent I_2-free quasi solid-state DSSCs. In addition, we have employed Raman spectroscopy to validate the in-situ generation of I_3^- ions in I_2-free polymer electrolytes alone and embedded in liquid-state DSSCs. Our observations on liquid-state DSSCs with only ILs, where these phenomena are much emphasized, encouraged us to develop QSSCs by using PILs ((poly(1-N-methylimidazolium-pentylpolydimethylsiloxane)iodide)) with different ionic functionality, ILs (MPII and MPITFSI), and their respective blends with and without I_2. and compare their performance and stability. As a result of optimization, we report here the highest PCE (8.3 % and 9.1% under 1 and 0.3 sun illumination), excellent long-term stability (only 16% efficiency loss after 26 months of aging), and improved transparency on quasi-solid state DSSCs based on I_2-free

PS3/EC polymer electrolyte and a traditional $TiCl_4$-treated randomly-organized TiO_2 + scattering layer.

2. Experimental section

2.1. Materials

The FTO glass substrate (TEC15) and the TiO_2 colloidal pastes (18 NR-AO) were purchased from Dyesol. Transparent TiO_2 electrodes (13 µm) were purchased from Greatcellsolar. Ti-Nanoxide R/SP paste, Platisol platinum solution, the N719 dye, and the Surlyn spacer (60 µm) were bought from Solaronix. Acetonitrile, iodine (I_2), 1-butyl-3-methylimidazolium iodide, guanidine thiocyanate, 4-tert-butylpyridine, valeronitrile, ethanol, titanium tetrachloride, ethylene carbonate (EC) and $LiClO_4$ were all obtained from Sigma Aldrich.

2.2. Fabrication of PILs-based electrolytes

The synthesis procedure of PILs and ILs is reported in our previous work.[75] The PILs, poly(1-N-methylimidazolium-pentylpolydimethylsiloxane)iodide having different ionicity and viscosity (denoted to PS1, PS2, and PS3 in this work), and the ILs, 1-methyl-3 propylimidazolium-iodide (MPII) and 1-methyl-3-propyl-imidazolium-Bis(trifluoromethane)sulfonimide (MPITFSI) were synthesized as reported elsewhere [75]. The polymer electrolytes (with and without I_2) were prepared by mixing the three synthesized PILs with the ILs or the EC. Electrolytes based on ILs (with and without I_2) were also prepared. Appropriate weights of the components (PILs, ILs, EC, and I_2) were dissolved in a very small amount of acetonitrile/valeronitrile (85/15, v/v) and then continuously stirred at 50 ^oC until complete dissolution (Table S1). The "reference" liquid electrolyte consisted of 0.6 M 1-butyl-3-methylimidazolium iodide, 0.03 M I_2, 0.1 M guanidine thiocyanate and 0.5 M 4-tert-butylpyridine in acetonitrile/valeronitrile (85/15, v/v).

2.3. Fabrication of DSSC

Prior to use, commercially TiO_2 photoanodes were sintered at 450 ^oC for 30 min. Additionally, a scattering layer (Dyesol 18 NR-AO) was deposited by spin-coating. In this work three types of photoanodes were used: the commercial-13 µm-TiO_2 photoanodes (marked as TiO_2 photoanodes), the commercial-13 µm TiO_2 photoanodes with an additional scattering layer of 4 µm (marked as TiO_2/SL photoanodes), and $TiCl_4$-treated commercial-13 µm TiO_2 photoanodes with additional scattering layer of 4 µm (marked as $TiCl_4$-TiO_2/SL photoanodes). The overall thicknesses of TiO_2/SL photoanodes were kept at approximately 17 µm (13 µm of mesoporous photoanode + 4 µm of scattering layer). The $TiCl_4$ treatment of the TiO_2/SL photoanodes was carried out by soaking the photoanodes in a 0.04 M $TiCl_4$ aqueous solution at 70 °C for 30 min. After rinsing in water and ethanol, the photoanodes were dried and sintered again in the air for 30 min at 450 °C. All freshly sintered photoanodes were immersed in N719 alcoholic solution at room temperature for 24 h. Finally, the dye-sensitized photoanodes were assembled in a sandwich configuration with a Pt counter-electrode and surlyn as a spacer. The electrolytes were vacuum backfilled into the device through the hole in the counter electrode. Before sealing, the device was heated at 100 ^oC for 5 min on a hot plate, followed by vacuum drying overnight to ensure the complete removal of volatile solvent. Finally, the hole was sealed with surlyn and a microscope cover glass.

2.*4. Characterization techniques*

The TiO_2 photoanode thicknesses and effective electrolyte infiltration were determined by scanning electron microscopy (FEG-SEM XL30, FEI). The pore-filling was asserted by cross-section energy-dispersive X-ray spectroscopy (EDX) elemental mapping of the device. Photocurrent-voltage *(J–V)* characteristics of the devices were measured by the solar simulator (from Newport Spectra-Physics) coupled with a Keithley 2400 Source Meter under a simulated Air Mass 1.5G solar spectrum (irradiance: 100 $mWcm^{-1}$, i.e. 1 sun). The area exposed to light

was 0.159 cm^2. Incident Photon to Charge Carrier Efficiency (IPCE) data was collected in the 300-800 nm range using a Xe lamp associated with a monochromator (Triax 180, Jobin Yvon). The integrated J_{sc} value was calculated from the IPCE based on ASTM G173-03 solar spectral irradiance (Global tilt Wm^{-2} nm^{-1})[76]. The open-circuit voltage decay (OCVD) measurements were achieved by illuminating the DSSC device with a white LED and then observing the voltage decay by the oscilloscope (Tektronix MDO3024) when the light source is turned off. Electrochemical impedance spectroscopy (EIS) was done using a BioLogic SP-200 potentiostat (Science Instrument), under dark conditions at room temperature, in the 10 mHz - 100 kHz frequency range by applying a bias equal to the V_{oc}. The obtained data were analyzed with the EC-lab software. Raman microprobe measurements were done using a HR800-UV Horiba-Jobin Yvon spectrometer coupled with an Olympus metallographic microscope. The measured spectra were obtained using as excitation the red line of the He–Ne laser (λ = 632.8 nm). The transmittance spectra of the devices and the diffusive reflectance spectra of the photoanodes were recorded using a UV-visible spectrophotometer (Perkin Elmer UV-Vis Spectrometer Lambda 14P). The absorbance spectra of the electrolytes were recorded using a UV-Vis spectrophotometer (Shimadzu 1600). A Biologic SP50 electrochemical workstation was utilized to assess the redox and the mass transfer capacity of the electrolytes through cyclic voltammetry (CV) and Tafel polarization measurements, respectively. The CV measurements for investigating reduction and oxidation processes in ILs and PILs/ILs were performed at 5 mV s^{-1} scan rate by using a three-electrode configuration with Pt (diameter = 3 mm) as a working electrode, Pt as a counter electrode, and Ag wire as a Pseudo-reference electrode. The measurement was carried out on neat ILs or PILs/ILs without any solvent and I_2 in Glove-box. The CV measurements were also performed at 50 mV s^{-1} scan rate by using a three-electrode setup with Pt as counter and working electrodes and Ag/AgCl (sat KCl) from Biologic (E_o = 0.197 vs NHE) as the reference electrode. The electrolyte was obtained by diluting 20 µL of

each electrolyte with 20 mL ACN containing 0.1M $LiClO_4$. The Tafel polarization plots were recorded at a scan rate of 10 mV s^{-1} by using a Pt-Pt parallel symmetric cell (distance in between = 2 mm) with the same electrolyte in between.

3. Results and discussion

3.1 Electrolyte design

All three PILs we have chosen have different ionic functionality (Fig. 1), leading to different ionic and physical properties as shown in Table S1[75]**.** The ionic conductivity of the neat ILs, PILs, PILs/ILs, and PIL/EC (with no solvent and I_2) was calculated from the bulk resistance obtained from the complex impedance plot as shown in Fig. S1 [5]. Considering these previous results, we selected only a few of the quasi solid-state electrolytes (PILs, PILs/IL, and PILs/EC) for the present study. Indeed, for DSSC fabrication, two ILs (MPII and MPITFSI) and a non-ionic liquid (EC) were used for the electrolytes preparation. The MPII acts as a source of I^- species whereas the MPITFSI mainly improves the conductivity.

The CV curves of the neat MPII are shown in Fig. S2a-b. In oxidation, due to the high concentration of the I^-, an oxidation wall can be noticed and the reduction of generated I_3^- is observed in the reverse scan. Regarding the stability in reduction, at around +600 mV, the reduction of I_3^- traces present in the electrolyte (a little oxidation of the electrolyte via O_2) is observed. At –1.1 V, the reduction of the imidazolium cation, due to its acidic proton, is observed [77]. During the return sweep, several oxidation processes can be observed, associated with the species obtained by reduction, but no oxidation can be obtained if the scan was stopped at -1 V vs Ag, indicating the purity of the used ILs.

As reported previously in our group [46,75], moderately (PS2) and highly (PS3) functionalized polymers show good compatibility with the imidazolium-based ILs and EC when added in large proportion, whereas PS1 is only miscible with MPITFSI due to its lower ionic functionality and hydrophobic character. However, we have demonstrated that in PS2/MPII/I_2 electrolytes the DSSCs performances were higher (PCE = 5.6%) due to the higher availability of I^- ions [46]. Therefore, this blend was further investigated in this work. Concerning the addition of EC, we opted for the most concentrated PIL, the PS3 which is rich in I^- as the addition of solvent reduces the ionic concentration. Furthermore, for this type of electrolyte, good photovoltaic performances are associated with the creation of ionic/non-ionic phase-separated domains that favor I^- percolation and rapid diffusion [78,79]. As shown in Fig. 1, for the highly substituted PS3/EC blends the hydrophilic domains are better defined and more continuous, facilitating the ion flow despite its high viscosity.

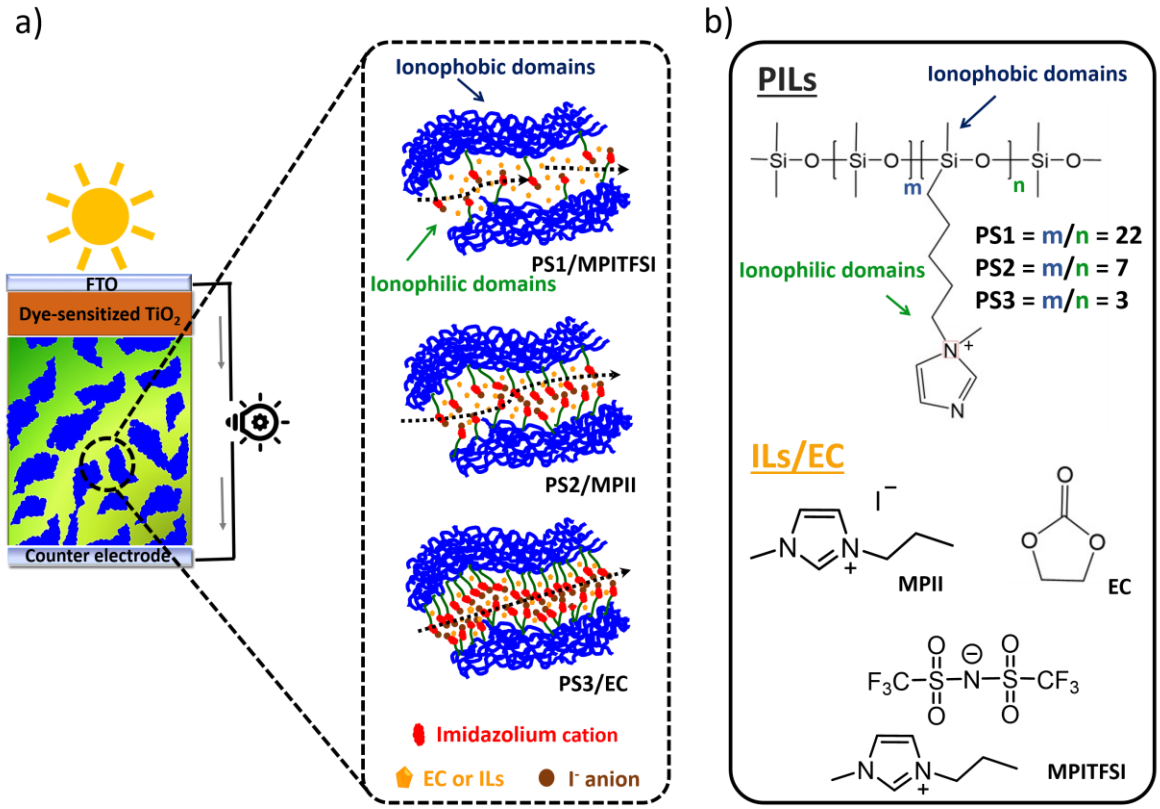

Fig. 1. (a) Schematic illustration at nanoscale level of the ions percolation paths through the hydrophilic domains in low (PS1), moderate (PS2), and highly (PS3) substituted PILs. (b) Chemical structures of poly(ionic liquid)s (PILs) having different ionic functionalities, ionic liquids (ILs), and ethylene carbonate (EC).

3.2. Photovoltaic performance of ionic liquid-based electrolytes

The *J*–*V* characteristics and photovoltaic parameters (V_{oc}: open-circuit voltage; J_{sc}: short-circuit photocurrent; FF: fill factor; PCE: overall power conversion efficiency) of the DSSCs using different I_2-based and I_2-free ILs and the commercial 13-μm TiO_2 photoelectrode are shown in Fig. 2a and Table 1.

Table 1. Photovoltaic parameters of the DSSCs on the 13-μm TiO_2 photoelectrode in combination with liquid, I_2-based, and I_2-free ILs-based electrolytes. The photovoltaic performance is the result of averaging 3-4 devices and standard deviation values are also included.

Device code	Electrolyte	V_{oc} (V)	J_{sc} (mA cm^{-2})	FF (%)	Average PCE (%)
D1	Reference (liquid)	0.66 ± 0.007	12.25 ± 0.42	68.37 ± 0.26	5.49 ± 0.22
D2	MPII	0.65 ± 0.01	13.02 ± 0.38	55 ± 0.97	4.64 ± 0.25
D2I	MPII/I_2	0.56 ± 0.01	9.87 ± 0.75	60 ± 0.74	3.28 ± 0.31
D3	MPITFSI	0	0	0	0
D3I	MPITFSI/I_2	0.39 ± 0.015	0.82 ± 0.04	51 ± 2.17	0.16 ± 0.016

As expected, the DSSC with MPITFSI (D3) did not generate a photocurrent since it had no redox mediator, whereas by adding I_2 (D3I) a little amount of I^- was formed, resulting in a working device (Table 1 and Fig. 2a). As expected, the large increase in I^- concentration, using the MPII/I_2 electrolyte (D2I) generated much higher V_{oc} and J_{sc} than its MPITFSI/I_2 counterpart. Interestingly, the omission of I_2 from MPII drastically improved J_{sc} and V_{oc} probably due to the difference between Fermi level of TiO_2 and redox potential of electrolyte [52] but led to a reduced FF due to a higher charge transport resistance associated with the insufficient amount of I_3^- [56,73]. It has been demonstrated that the imidazolium-based IL could be used as the sole charge transfer mediate [80]. Without I_2, I_3^- can be formed by the

reaction of I^- with the oxidized dye (dye^+) (step 1), and then I^- ions were regenerated by a reduction process at the counter electrode (step 2).

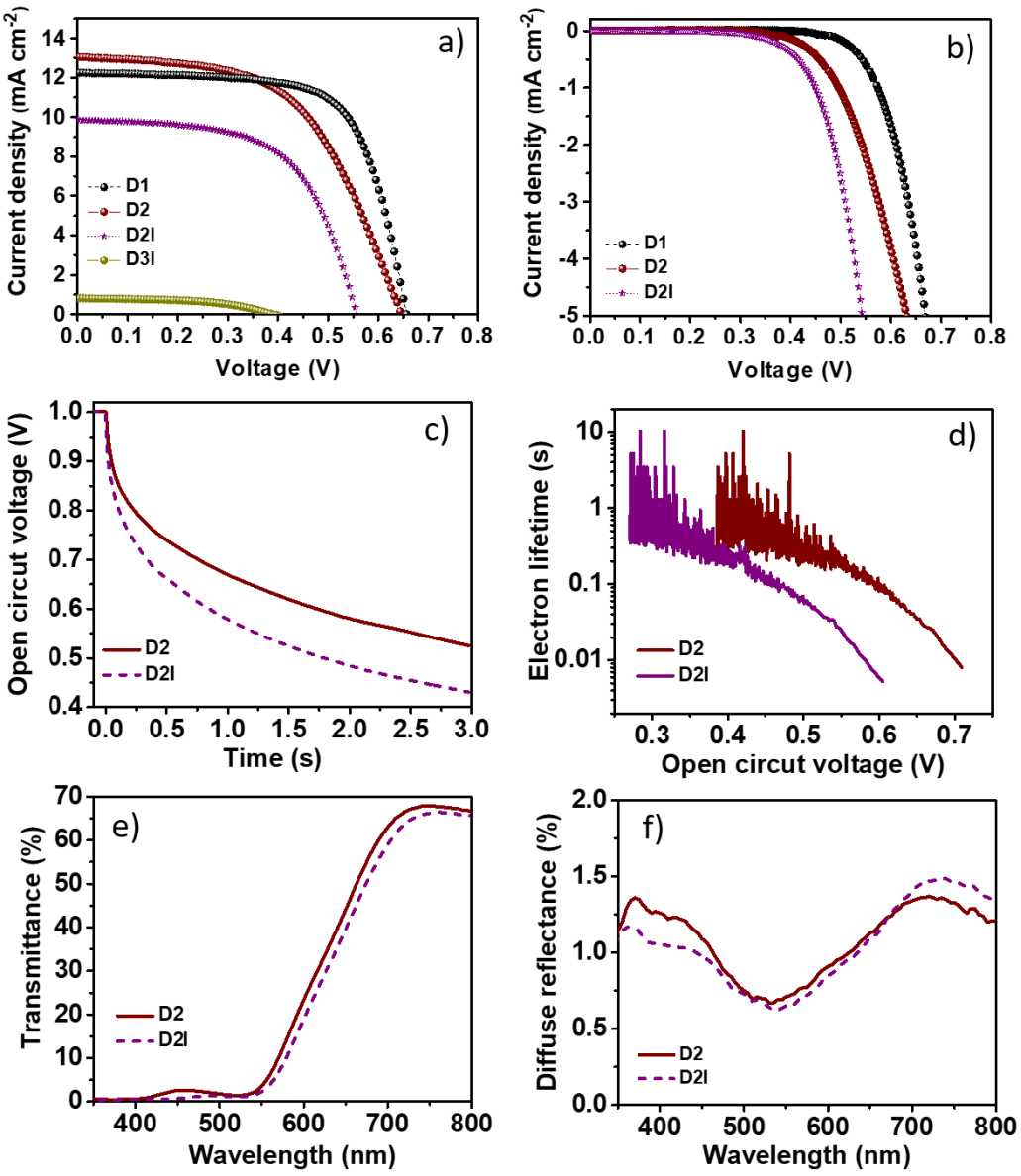

Fig. 2. *J-V* curves of the DSSCs comprising a 13-μm TiO_2 photoelectrode in combination with liquid, I_2-based, and I_2-free ILs-based electrolytes under 1 sun (a) and in dark (b); the OCVD measurements (c) and calculated electron lifetime (d) of I_2-based and I_2-free DSSCs under white LED, the transmittance (e) and the diffuse reflectance (f) spectra of the I_2-based and I_2-free DSSCs. See Table 1 for DSSC codes.

$$3I^- + 2\,dye^+ \longrightarrow I_3^- + 2\,dye \quad \text{(step 1)}$$

$$I_3^- + 2\,e^- \longrightarrow 3I^- \quad \text{(step 2)}$$

$$I^- + I_2 \longrightarrow I_3^- \longrightarrow \text{polyiodides}$$

The enhanced V_{oc} for I_2-free MPII is correlated with the suppression of the dark current at the TiO_2 /electrolyte interface (Fig. 2b). The presence of extra I_2 in the electrolytes leads to the formation of polyiodides such as I_5^- and I_7^- which can recombine with the electrons from the photoanode conduction, resulting in an increase of the dark current. Zaban et al. [81] reported that the charge recombination process and electron transport properties play an important role in improving V_{oc} and J_{sc}. It has been reported that the OCVD measurements can provide the information about recombination process and electron lifetime in solar devices [82,83]. As shown in Fig. 2c, the I_2-free device (D2) had a milder decay measured as compared to the I_2-based device (D2I), indicating a reduced charge recombination effect. The electron lifetime (τ_e) is defined by using equation 1 [84]:

$$\tau_e = -\frac{k_B\,T}{q} \Big/ \left(\frac{dV_{oc}}{dt}\right) \qquad (1)$$

Where k_B is the Boltzmann constant, T is the absolute temperature in kelvin and q is the elementary charge. The results showed that the calculated electron lifetime is higher for the I_2-free device (D2) as compared to I_2-based (Fig. 2d), indicating the reduced surface traps and charge recombination. Developing highly transparent DSSCs makes them suitable for greenhouse-oriented and BIPV windows applications, and provides better aesthetics [67,69,71]. The transmittance spectra of D2 was blue-shifted with the report to D2I (Fig. 2e)

as a sign of improved light harvesting, which is in perfect agreement with the enhanced J_{sc}. To examine the visible light absorption of MPII/I_2 and MPII electrolytes (both 10x diluted with acetonitrile/valeronitrile), the UV-VIS spectra were measured. As shown in Fig. S3, the I_2-free MPII looks colorless and absorbs less visible light compared to the one with I_2 [85]. Fig. 2f also showed that the D2 exhibited higher diffuse reflectance than the D2I, indicating that light penetrated deeper into the structure of dye-sensitized TiO_2 leading to multiple internal reflections and thus more effective charge photogeneration.

We used Raman spectroscopy to investigate the iodide speciation in MPII and MPII/I_2 electrolytes and corresponding devices under constant cell illumination. As shown in Fig. 3a the MPII/I_2 electrolytes exhibited a peak at around 116 cm^{-1} representing the symmetric stretch vibration of I_3^- [56,86] (noted with Peak 1) and a second prominent peak centered at around 152 cm^{-1} corresponding to the presence of polyiodides (noted as Peak 2) [87]. There was no indication of the presence of molecular I_2 which bands should appear around 180 cm^{-1} [87]. The Raman spectra of I_2-free MPII electrolyte showed no bands confirming the absence of I_3^-. In which concerns the corresponding devices, the 116 cm^{-1} band was identified in both devices and particularly in the I_2-free MPII, indicating the in-situ generation of I_3^-. A peak centered at 146 cm^{-1} (noted as Peak 3 in Fig. 3a) could be assigned to the N719 sensitized TiO_2 [88]. Increasing the measurement time seemed to not affect the Peak 1 and Peak 3 evolution (Fig. 3b) indicating that the I_3^- was constantly generated and regenerated as well as the polyiodides whose contribution was observed at around 170 cm^{-1} (peak 4) [88]. The evolution of the Peak 3/Peak 1 ratio confirmed that an equilibrium, not far from the initial state, of the I_3^- flow inside the device, was quickly established through the Grotthuss-type electron exchange mechanism [89].

Contrarily, in the case of the D2I device, Peaks 1 strongly evolved with the report to Peak 3 (Fig. 3c) as the analysis time was increased. The intensity of Peak 1 with the report to Peak 3

markedly decreases in the first 8 to 10 min (Fig. 3d) indicating an initial system overload with I_3^-. It is very likely that part of the I_3^- species no longer interacted with the dye but were completely reduced to I^-. The absence of polyiodides in the iodide-containing might be due to the same spontaneous reduction process encouraged by a possible functioning in over operando conditions ($V_{oc\ D2I} < V_{oc\ D2}$, Table 1) [88].

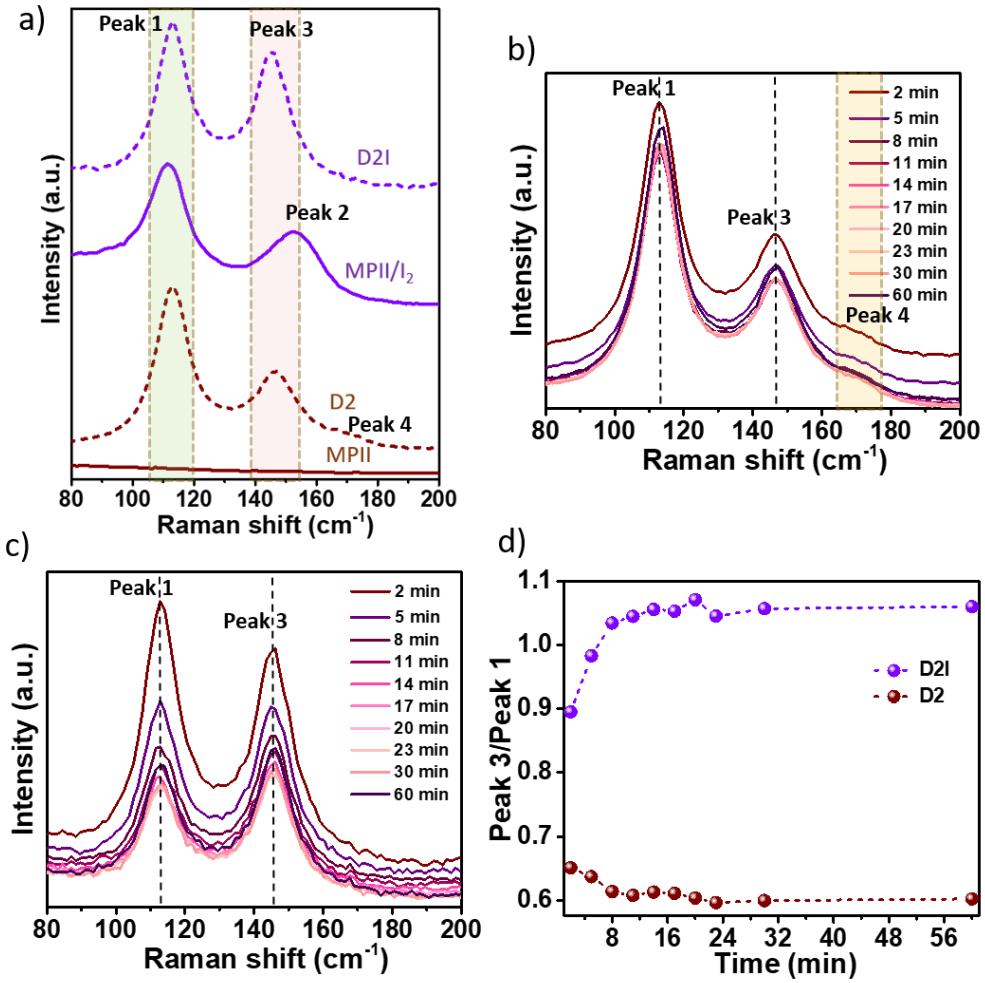

Fig. 3. (a) Raman spectra of MPII, MPII/I_2, D2, and D2I recorded after 2 mins of laser illumination. Raman spectra of (b) device D2 and (c) device D2I were recorded during different time intervals. Colors change from wine to violet with time. (d) Evolution of the Peak 3 (dye-sensitized TiO_2) to peak 1 (I_3^-) intensities ratio as a function of time.

3.3. Photovoltaic performance of polyionic liquid-based electrolytes

Then, DSSCs prepared with the PS1, PS2, and PS3 PILs electrolytes were investigated. First of all, devices (D4, D4I, D5, and D5I) fabricated with the least viscous PS1 result in poor efficiencies and the addition of MPITFSI further degrades the efficiency by lowering the I^- concentration despite the higher ionic conductivity (Table S2 and Fig. S4a). The I_2-free device (D4) showed the highest, still modest, efficiency in agreement with the higher photon harvest and conversion efficiency (Fig. S4b) and lower dark current (Fig. S5a). The PS2 and PS3 are very viscous (106 and 1071 Pa s, respectively), having slow diffusion coefficients, which represents the main drawback in applications like DSSCs [90]. We tried to improve this aspect by blending them with MPII and EC [46]. As shown in Fig. 4a and Table 2, PCE values of 3.42% and 4.50% were achieved for the PS2/MPII/I_2 and PS3/EC/I_2 devices, respectively when using the same commercial 13-μm TiO_2 photoelectrode. Higher V_{oc} and J_{sc} values were calculated for the I_2-free D6 and D7 devices in comparison with their counterparts in part due to the increase of the potential difference between the TiO_2 fermi level and the electrolyte redox level, but also due to the improved light-harvesting once the I_2 absorption was removed (Fig. S3b). The higher V_{oc} of the I_2-free D7 device compared to D6 is related to the polymer electrolyte's higher ionic conductivity (Table S1) and thus lower viscosity which improved interface contact.

Table 2. Photovoltaic parameters of the DSSCs on the 13-μm TiO_2 photoelectrode in combination with I_2-based and I_2-free PS2 and PS2/MPII based electrolytes

Device	Electrolyte	V_{oc} (V)	J_{sc} (mA cm^{-2})	FF (%)	PCE (%)
D6	PS2/MPII	0.67 ± 0.007	10.94 ± 0.38	61 ± 0.74	4.47 ± 0.25
D6I	PS2/MPII/I_2	0.63 ± 0.01	8.44 ± 0.45	64 ± 2.09	3.42 ± 0.31
D7	PS3/EC	0.71 ± 0.01	11.68 ± 0.45	60 ± 1.17	5.03 ± 0.32
D7I	PS3/EC/I_2	0.65 ± 0.01	10.77 ± 0.45	65 ± 0.16	4.50 ± 0.17

The device D7 based on the I_2-free PS3/EC showed the highest J_{sc} and V_{oc} (Table 2 and Fig. 4a), a FF of 60%, resulting in the highest PCE, 5.03%, and improved transparency (Fig. S3b). The solid nature of PS2 and PS3 was not changed either with the addition of MPII or EC (Fig. S3a).

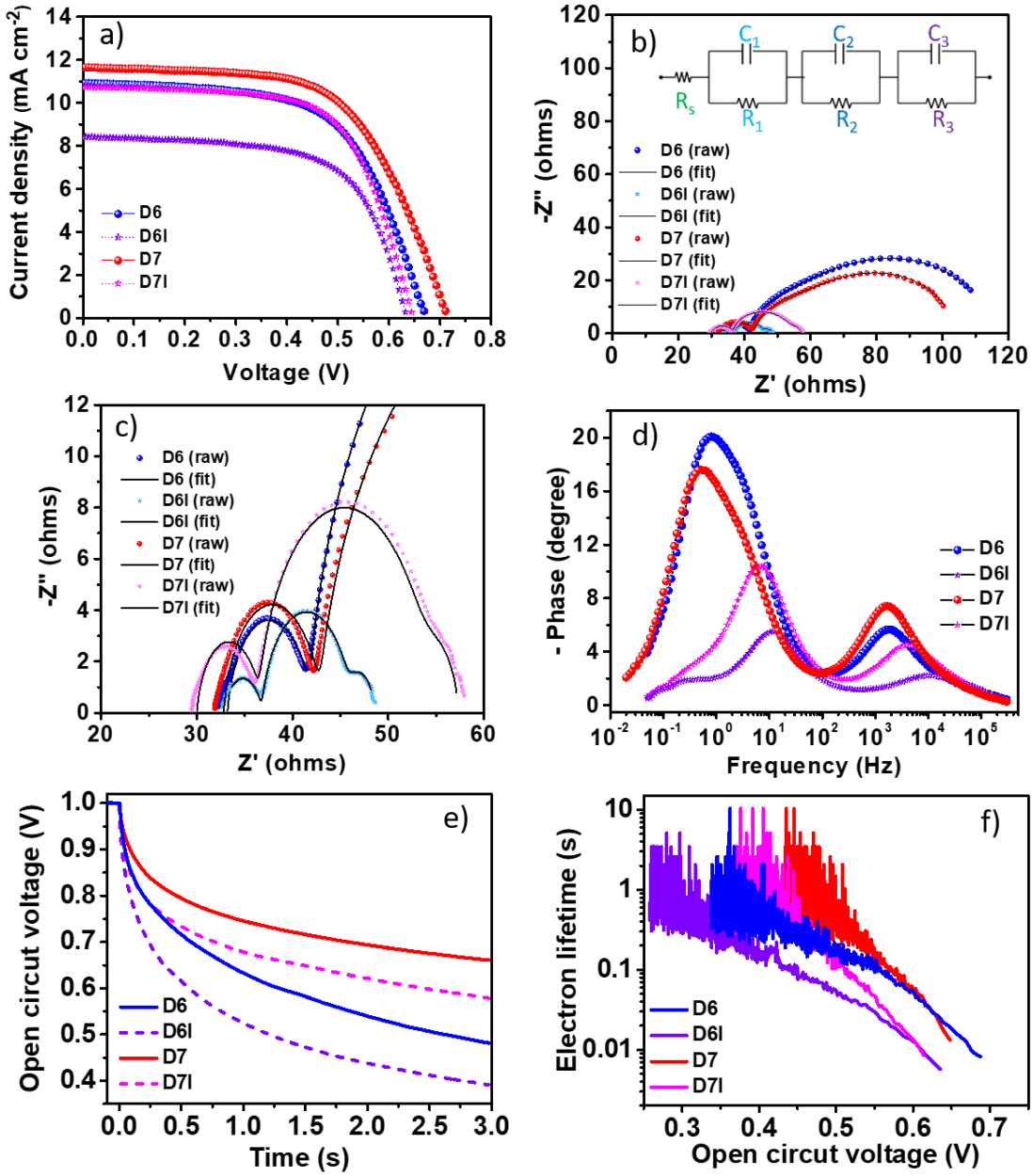

Fig. 4. (a) J-V of DSSCs comprising a 13-µm TiO_2 photoelectrode in combination with I_2-based and I_2-free PS2/MPII and PS3/EC-based electrolytes. (b) Full EIS Nyquist plot and the circuit used for fitting, (c) zoomed EIS Nyquist plot, (d) the Bode phase plots measured in dark for the DSSCs with different electrolytes, and (e-f) the OCVD measurements and calculated electron lifetime of I_2-based and I_2-free DSSCs. See Table 2 for DSSC codes.

As previously mentioned the V_{oc} and J_{sc} should increase when I_2 is removed from the electrolyte. Indeed, the highest V_{oc} value is obtained for the I_2-free electrolytes (Table 2), which agrees with the dark current diminution (Fig. S5b) but also with the electrochemical results. Upon blending the MPII to PS2, the slope of the oxidation of I^- in I_3^- is lower for PS2/MPII due to the higher viscosity (Fig. S6).

To prove our V_{oc} increase hypothesis, we have evaluated the redox capacity of our electrolytes through CV. The CV curves of PS2/MPII and PS2/MPII/I_2 were prepared in 0.1 M $LiClO_4$ in ACN. (Fig. S7a) reveal the presence of two anodic peaks at around 0.7/0.9V and 0.4/0.5V vs. Ag/Ag^+ (E_{pa}^1 and E_{pa}^2, respectively in Table S3) corresponding to the I^-/I_3^- and I_3^-/I_2 redox reactions.

The E_{pa}^1 and E_{pa}^2 and the corresponding cathodic E_{pc}^1 and E_{pc}^2 calculated values were used to determine the electrolyte formal redox potential E_0 vs NHE = $(E_{pa} + E_{pc})/2 + 0.197$. The values are gathered in Table S3 and also represented in Fig. 5 for the I_2-free and I_2-containing PS2/MPII electrolytes. Indeed, the V_{oc} of I_2-free PS2/MPII electrolyte is higher than its iodine-rich counterpart and higher than the standard iodide electrolyte, explaining the higher J_{sc} and PCE values. The more anodic redox potential of the PS2-based electrolytes also enhances the dye regeneration rate.

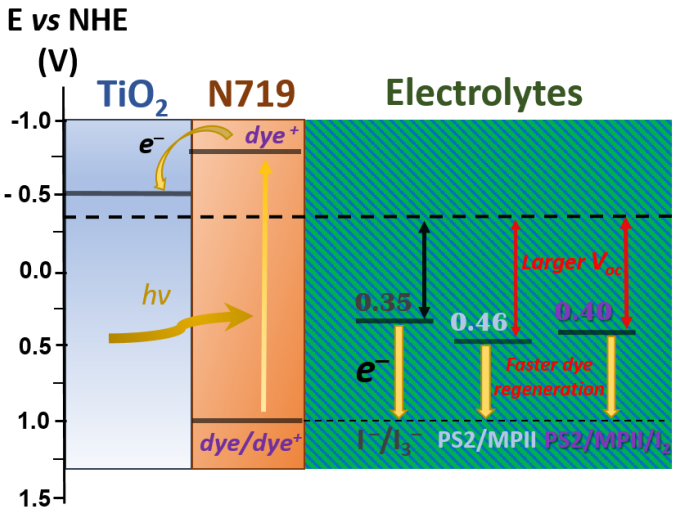

Fig. 5. Energy level diagram for the PS2/MPII and PS2/MPII/I_2 electrolytes.

Tafel polarization curves were performed in a Pt-Pt symmetrical cell containing the same electrolyte and allowed determining the exchange (J_0) and diffusion-limited (J_{lim}) current densities as indicated in Fig. S7b. The limiting current is attributed to the maximum ionic carrier transfer and allows calculating the apparent diffusion coefficient D_{app} using the following equation [5]:

$$D_{app} = dJ_{lim}(2nFC)^{-1} \qquad (2)$$

In equation 2, *d* is the electrodes gap (2 mm), *n* is the number of electrons involved in the reduction of the I_3^- reaction which is 2, *F* is the Faraday's constant (96485.4 C mol^{-1}) and *C* is the concentration of I_3^-. The electrolyte/Pt charge transfer resistance R_{ct} can be determined based on J_0 values by using the following equation [91]:

$$J_0 = RT/nFR_{ct} \qquad (3)$$

Here *n* is the number of electrons transferred which is 2; *F* is the Faraday constant, *R* is the gas constant (0.082 $L{\cdot}atm{\cdot}K^{-1}{\cdot}mol^{-1}$) and *T* is the absolute temperature (291.15 K). Since we used

the same Pt counter-electrodes the R_{ct} values will reflect the differences in the electrolyte ionic transfer properties. The J_{lim}, J_0, D_{app}, and R_{ct} values are listed in Table 3.

Table 3. Charge transfer characteristics of the PS2/MPII and PS2/MPII/I_2 electrolytes.

Electrolyte	J_{lim} (10^{-2} mA cm^{-2})	J_0 (10^{-3} mA cm^{-2})	D_{app} (10^{-6} cm^2 s^{-1})	R_{ct} (Ω cm^{-2})
PS2/MPII	13.49	0.6	0.90	195
PS2/MPII/I_2	15.84	1.8	1.05	68

As expected, the iodine-rich polymer has a higher J_{lim} due to the higher concentration of generated I_3^-. The removal of iodine does not severely impact the mass transfer properties of the PS2/MPII electrolyte as the D_{app} parameter is only slightly decreased (Table 3). The lower J_0 and thus higher R_{ct} values are a reflection of the lower ionic conductivity of the I_2-free PS2/MPII [46]. Nevertheless, the more anodic redox potential of the I_2-free electrolyte (Fig. 5) increases V_{oc} outcomes these effects leading to an increased PCE for the device based on I_2-free PS2/MPII electrolyte (Table 2). The R_{ct} values evolution from Tafel measurements was confirmed through electrochemical impedance spectroscopy (EIS).

The Nyquist and Bode phase plots of the DSSCs comprising polymer electrolytes are shown in Fig. 4b-c and 4d, respectively. The EIS spectrum of the DSSC is comprised of three signatures in the studied frequency range (10 mHz to 100 kHz) [92] and was fitted with the circuit illustrated in the inset of Fig. 4b. The first (high frequency) and second (middle frequency) semicircles correspond to the charge-transfer resistances at the counter electrode/electrolyte interface (R_1 and C1 are the resistance and capacitance of the corresponding double layer) and at the photoanode/electrolyte (R_2 and C_2 are the resistance and capacitance of the corresponding double layer) interfaces, while the third one in the low-

frequency range corresponds to the diffusion of the electrolyte (R_3 and C_3 are the electrolyte diffusion resistance and capacitance). The values of the circuit elements obtained through fitting are gathered in Table 4. The sheet resistance (R_s) comprises the contacts/wires and electrolyte resistance. The lower R_s value of I_2-based electrolytes for DSSCs explained the slightly better FF [56,71,72,93]. A lower R1 and R_2 for the I_2-containing electrolytes versus the I_2-free counterparts was correlated to the higher concentration of I^-/I_3^- at the photoanode interface [56,71]. Nevertheless, this can be a negative point for the DSSCs as excess I_3^- can induce parasitic/recombination reactions. However, the extremely large R_3 value of the I_2-free electrolytes-based DSSCs indicated a very little amount of I_3^- ions as the EIS measurements were done in dark conditions [56,71]. The effective electron lifetime (τ_e) was calculated from the bode phase plot (Fig. 4d) based on the lower frequency range peak by using equation 4 [94]:

$$\tau_e = \frac{1}{2\pi f_{max}} \quad (4)$$

Where f_{max} is the frequency of the peak. The I_2-free DSSCs have a superior electron lifetime than the one with I_2 – containing counterparts (Table 4). Likewise, the V_{oc} decay rate (Fig. 4e) and the calculated electron lifetime (Fig. 4f) of the DSSCs with I_2-free electrolyte were much higher than for the ones with I_2-based DSSCs, in agreement with the EIS measurements. This further confirms that the charge recombination is suppressed by the removal of I_2 from polymer electrolytes with a better effect for the D7 device which is our champion device. The decrease in charge recombination is also consistent with the diminution of the measured dark current (Fig. S5b).

Table 4. Parameters were obtained by fitting the EIS spectra of the DSSCs incorporating different electrolytes.

Device	Electrolyte	R_s (Ω)	R_1 (Ω)	R_2 (Ω)	R_3 (Ω)	f_{max} (Hz)	τ_e (ms)
D6	PS2/MPII	33	9	20	53	0.81	197
D6I	PS2/MPII/I_2	31	4	9	3	12.87	13
D7	PS3/EC	33	10	21	40	0.53	300
D7I	PS3/EC/I_2	30	7	17	4	7.27	22

We have disassembled the D7 device upon the completion of the above-referred examination of the PV performances. The cross-section SEM analysis (Fig. S8a) confirmed that the polymer infiltrated thoroughly the pores of TiO_2 (grain boundaries not visible) and evenly covers the entire TiO_2 photoanode, ensuring good interfacial contact, excellent pore-filling, and thus efficient dye regeneration. The EDX spectrum (Fig. S8b) confirmed the presence of titanium (Ti), silicon (Si), and iodine (I) through the entire cross-section, while the mapping illustrated in Fig. S8c confirmed the electrolyte penetration across the TiO_2 photoanode thickness.

3.4. Influence of scattering layer

So far, we assessed the photovoltaic performance of the DSSCs based on the PS3/EC (D7) and PS3/EC/I_2 (D7I) electrolytes with thicker photoelectrode. A light scattering layer (SL) of 18NR-AO of about 4 µm was deposited on top of the 13 µm photoelectrode to enhance the thickness and the light-harvesting. The cross-sectional SEM image in Fig. 6a showed that the TiO_2/SL photoanode is around 17 µm thick. By adding the SL, the diffuse reflectance of the

photoanode was increased (Fig. 6b). The J-V characteristics of all the devices made with TiO_2/SL photoanode and different electrolytes are shown in Fig. 6c, and their respective photovoltaic parameters are briefed in Table 5. In DSSCs, the impact of SL is largely retrieved in the J_{sc} value [95,96]. The ss-DSSCs with TiO_2/SL photoanodes showed superior PCE as compared to pristine TiO_2 photoanodes (Table 2 vs. Table 5). The J_{sc} is increased upon increasing the thickness, with a slight decrease in the FF. Notably, the device D7-SL (I_2-free PS3/EC in combination with TiO_2/SL photoanodes) showed the highest J_{sc} (14.94 mA cm^{-2}) corresponding to a 1.2 times improvement in efficiency compared to the device D7 (with commercial TiO_2 photoanodes). As shown in Fig. 6d, the maximum bandwidths of the IPCE spectra for PS3/EC DSSC (D7) were nearly the same as those of the PS1 DSSC (D4) but the plateau was much higher, which is consistent with the improved J_{sc}. For this device, the highest V_{oc} value was obtained which corresponded to a reduced dark current (Fig. S5c).

Table 5. J-*V* characteristics of DSSCs comprising a 17-μm TiO_2/SL photoelectrode combination with I_2-based and I_2-free PS2/MPII and PS3/EC -based electrolytes.

Device	Electrolyte	V_{oc} (V)	J_{sc} (mA cm^{-2})	FF (%)	PCE (%)
D6-SL	PS2/MPII	0.63 ± 0.004	14.03 ± 0.36	60 ± 1.39	5.30 ± 0.23
D6I-SL	PS2/MPII/I_2	0.59 ± 0.003	11.31 ± 0.55	61 ± 0.91	4.10 ± 0.21
D7-SL	PS3/EC	0.69 ± 0.005	14.94 ± 0.16	58 ± 0.83	5.97 ± 0.16
D7I-SL	PS3/EC/I_2	0.61 ± 0.007	13.34 ± 0.59	62 ± 0.76	5.04 ± 0.13

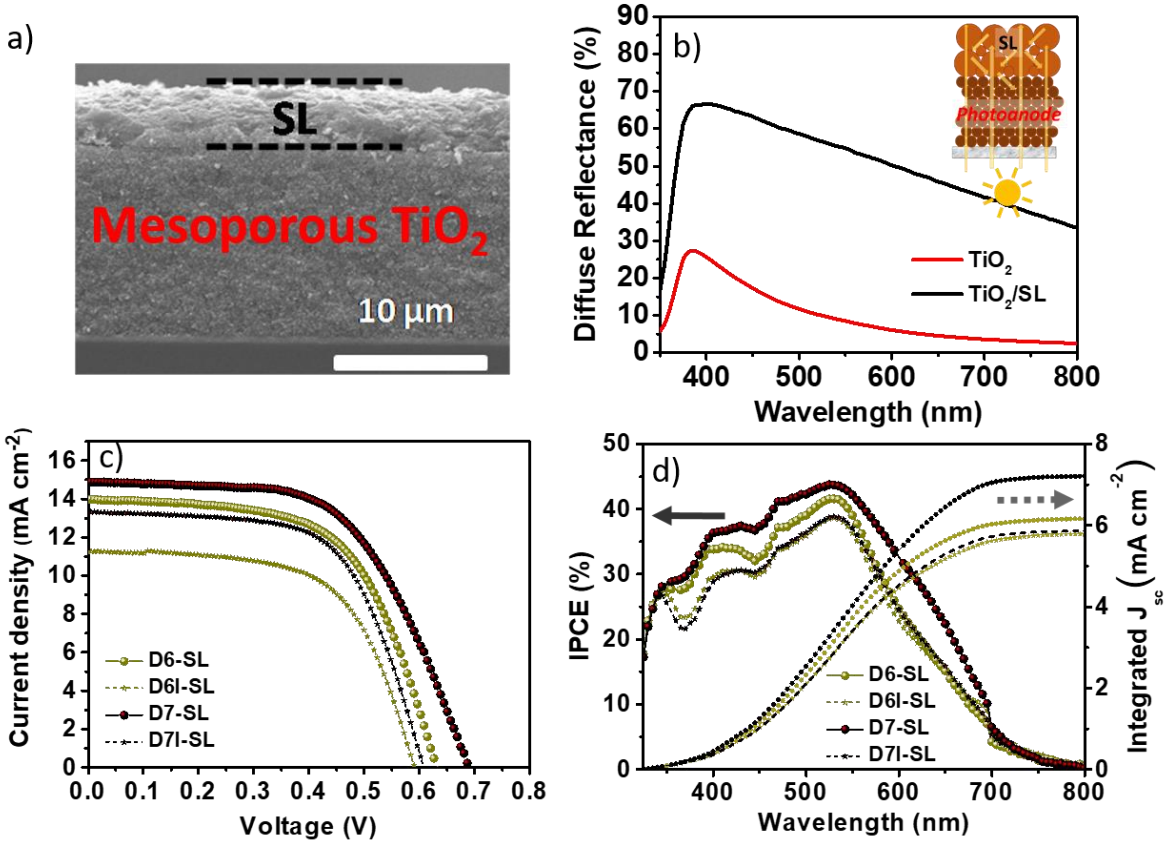

Fig. 6. (a) Cross-sectional SEM image showing double-layer structure TiO_2/SL photoelectrode; (b) diffuse reflectance of TiO_2 and TIO_2/SL photoanodes (insert shows a schematic drawing of a double layer structure photoelectrode formed by a nanocrystalline film and a light scattering layer on top); (c) J-V and (d) IPCE curves with integrated J_{sc} values of DSSCs comprising a 17-µm TiO_2/SL photoelectrode combination with I_2-based and I_2-free PS2/MPII and PS3/EC-based electrolytes. See Table 4 for DSSC codes.

3.5. Influence of $TiCl_4$ treatment

$TiCl_4$ post-treatment of TiO_2 photoanode significantly improves the photovoltaic performance of liquid electrolyte-based DSSCs as shown in Fig. S9. One of the reasons for improved performance is attributed to the increased surface area of the photoanode as a result

of $TiCl_4$ treatment, resulting in more dye loading and hence improved light-harvesting efficiency (Fig S10)[97]. To optimize the ss-DSSC performance, the TiO_2/SL photoanodes of the D7 and D7I devices were subjected to a post-treatment with aqueous 0.04M $TiCl_4$ at 70 ^oC for 30 min. The corresponding photovoltaic parameters are listed in Table 6 and Fig. 7a. The performance of the DSSC containing I_2-free highly substituted PS3/EC (D7-SL-$TiCl_4$) electrolytes was, boosted, yielding the highest efficiency ever reported for this type of electrolytes, 8.30%. In comparison, the device D7I-SL-$TiCl_4$ with PS3/EC/I_2 shows a relatively lower PCE of 6.50%. The combined effect of $TiCl_4$ and SL resulted in shifting the entire IPCE curve upward (Fig. 6d vs Fig. 7b). The performance improvements could be attributed to the improved connectivity between the TiO_2 grains, a shift in the conduction band edge of the TiO_2, reduced defect traps, and inhibition of electron recombination due to $TiCl_4$ treatment (Fig. S5d) [97–99]. We also believe that the extra dye-loading capacity provided by the $TiCl_4$ treatment, (Fig. S10) lead to an improved charge carriers photogeneration. It is also worth mentioning that ultrasound soldering of the electrode contacts improved the electric contacts, which resulted in DSSCs with high FF and PCE. The V_{oc} decay rate (Fig. 7c) and calculated electron lifetime (Fig. 7d) of the device D7I-SL-$TiCl_4$ were greater than its I_2-containing counterpart. The optimized D7-SL-$TiCl_4$ device under varied light intensity illumination (1 sun to 0.1 sun). Fig. 7e shows that the device maintained its performance even at low light intensity illumination (Table S4), with a maximum PCE value reaching 9.1% under 0.3 sun i.e. 30 mW cm^{-2}. DSSCs are mostly designed for indoor applications. Therefore, we studied the long-term stability of our best devices, D7-SL-$TiCl_4$ versus the D7I-SL-$TiCl_4$ by aging them in ambient conditions for 26 months. Astonishingly, D7-SL-$TiCl_4$ displayed excellent long-term stability, retaining up to 84% of its initial efficiency after 26 months, whereas the D7I-SL-$TiCl_4$ device retained only 23% (Fig. 7f and Fig. S11). This result further confirms the enhancement of the long-term stability of DSSC when fabricated with I_2-free polysiloxane electrolytes. We examined the

influence of SL thickness of two different SLs (18NR-AO and R/SP) on the photovoltaic output. The side-view images shown in Fig. S12 indicate that the 18NR-AO comprises small nanorods (~20 nm) mixed with large crystals (200-400 nm) and the R/SP paste contains only large nanoparticles (>100 nm) as also reported by Lan et al., [95]. Table S5 and Fig. S13 present the photovoltaic parameters showing the maximum performance obtained for 17 µm thickness for both AR-NO and R/SP SL which is attributed to the higher dye uptake (Fig. S10) and improved light-harvesting harvesting due to the superior light scattering (Fig. S12c-d). Note that the thicker TiO_2/3SL (19 µm) shows much lower performance than the others due to mass transportation limitations [100].

Table 6. Photovoltaic parameters of the DSSCs containing PS3/EC and PS3/EC/I_2 in combination with $TiCl_4$-TiO_2/SL photoanodes.

Device	Electrolyte	V_{oc} (V)	J_{sc} (mA cm^{-2})	FF (%)	PCE (%)
D7-SL-$TiCl_4$	PS3/EC	0.70 ± 0.004	19.40 ± 1.89	61 ± 1.77	8.30 ± 0.27
D7I-SL-$TiCl_4$	PS3/EC/I_2	0.64 ± 0.01	15.35 ± 0.45	66 ± 0.35	6.50 ± 0.30

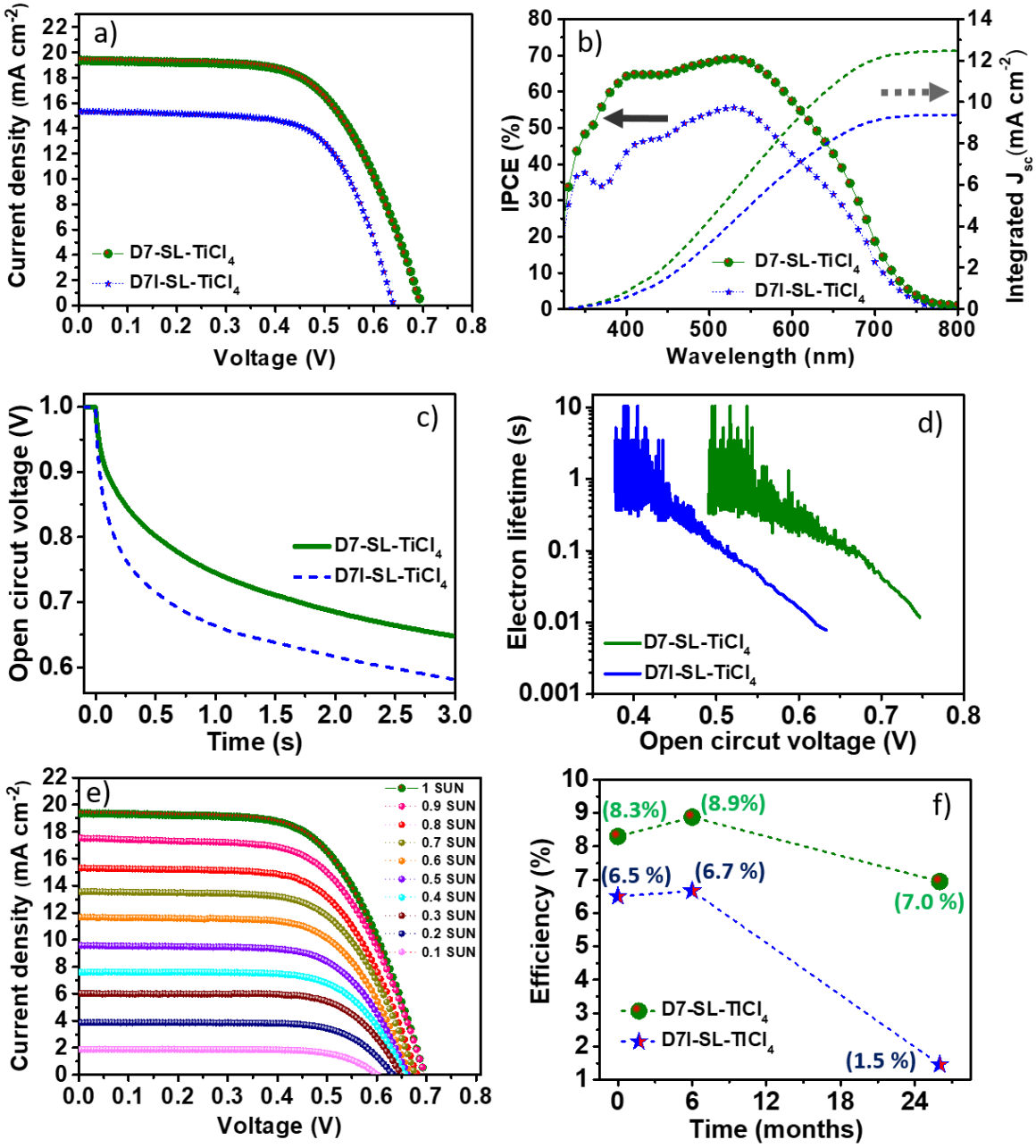

Fig. 7. (a) J-V and (b) IPCE curves with integrated J_{sc} values of DSSCs comprising a $TiCl_4$-TiO_2/SL photoelectrode combination with I_2-based and I_2-free PS3/EC and PS3/EC/I_2; the OCVD measurements and calculated electron lifetime of I_2-based and I_2-free DSSCs under white LED (c-d); (e) Photovoltaic parameters of the DSSCs containing $TiCl_4$-TiO_2/SL photoanode and I_2-free PS3/EC under 1 sun illumination; and (f) Evaluation of the long-term. stability of the I_2-based and I_2-free DSSC over 26 months. See Table 5 for DSSC codes.

Tables S6, S7, and S8 display the yearly evolution of the photovoltaic parameters of the all-state DSSCs based on polysiloxane, I_2-free, and PIL electrolytes, respectively. The careful examination of these data, reveals that the PCE reported in this work is higher than the efficiency reported for all-state I_2-free PILs and polysiloxane-based electrolytes, as highlighted in Fig. 8.

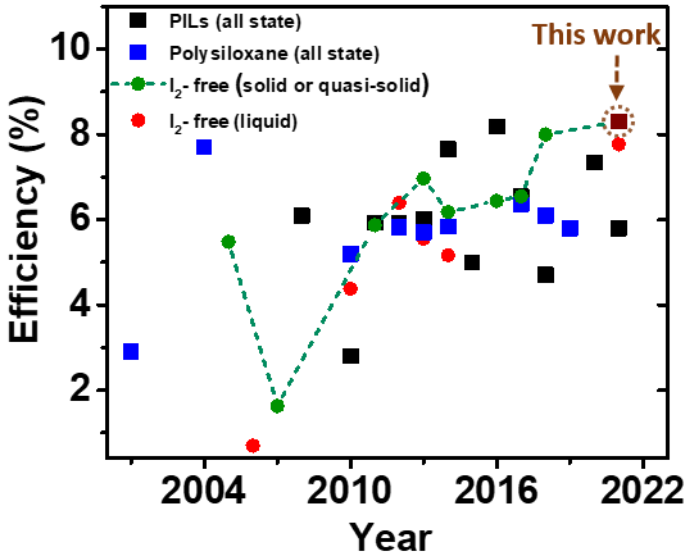

Fig. 8. Time evolution of the photovoltaic efficiency for the all-state DSSCs based on PILs, polysiloxane, and presence or absence of elemental I_2. See tables in supporting information for references.

4. Conclusion

A series of I_2-free polysiloxane-based poly(ionic liquids), having different ionic functionality and ionic liquids, as well as their blends, were successfully implemented as polymer electrolytes for quasi solid-state DSSCs. In this work, we have proved that exclusion of I_2 was necessary to diminish the polyiodide originated recombination, and thus enhance the transparency, photovoltaic performance, and device stability. Raman spectroscopy was used to prove the in-situ generation and efficient regeneration of I_3^- in I_2-free DSSCs but also to indicate the participation of polyiodide species in the charge transfer mechanism. Likewise, through this method, we identified the presence of excess I_3^- and its imperfect regeneration explaining the lower performance and stability of the I_2-containing devices. We have also shown through electrochemical analysis that the iodine removal increased the V_{oc} contributing to a more efficient charge photogeneration and dye regeneration.

Through electrolyte optimization, we have found that the highly substituted I_2-free PS3 polymer electrolyte plasticized with ethylene carbonate reached the highest reported efficiency (8.3 % and 9.1% under 1 and 0.3 sun illumination), excellent long-term stability (only 16% efficiency loss after 26 months aging) and improved transparency when tested with a traditional $TiCl_4$-treated randomly-organized TiO_2 with scattering layer.

We may, hence, anticipate that this work will trigger further interest in I_2-free polymer electrolytes and thus consolidate our efforts to develop stable and fully transparent efficient solar energy conversion devices while being extendable to other energy-related applications such as solar energy storage, photo-chargeable batteries.

Acknowledgments

The research was supported by ARC4-Énergies Région, Rhône-Alpes. The authors would also like to acknowledge IDS FunMAT (International Doctorate School in Functional

Materials) and the Centre of Excellence of Multifunctional Architectured Materials "CEMAM" n° AN-10-LABX-44-01 for financial support. Electron microscopy studies were performed at the CAREM facility (Celluled'Appui à la Recherche et à l'Enseignement en Microscopie - ULiège).

References

[1] A. Fujishima, K. Honda, Electrochemical photolysis of water at a semiconductor electrode, Nature. 238 (1972) 37–38.

[2] B. O'Rdgan, M. Gratzel, A low-cost high-efficiency solar cell based on dye-sensitized colloidal TiO2, Nature. 353 (1991) 737–739.

[3] Y. Cao, Y. Liu, S.M. Zakeeruddin, A. Hagfeldt, M. Grätzel, Direct contact of selective charge extraction layers enables high-efficiency molecular photovoltaics, Joule. 2 (2018) 1108–1117.

[4] J.V. Vaghasiya, K.K. Sonigara, S.S. Soni, S.C. Tan, Dual functional hetero-anthracene based single component organic ionic conductors as redox mediator cum light harvester for solid state photoelectrochemical cells, J. Mater. Chem. A. 6 (2018) 4868–4877.

[5] K.K. Sonigara, H.K. Machhi, J.V. Vaghasiya, A. Gibaud, S.C. Tan, S.S. Soni, A smart flexible solid state photovoltaic device with interfacial cooling recovery feature through thermoreversible polymer gel electrolyte, Small. 14 (2018) 1800842.

[6] D. Devadiga, M. Selvakumar, P. Shetty, M.S. Santosh, Recent progress in dye sensitized solar cell materials and photo-supercapacitors: A review, J. Power Sources. 493 (2021) 229698.

[7] M. Kokkonen, P. Talebi, J. Zhou, S. Asgari, S.A. Soomro, F. Elsehrawy, J. Halme, S. Ahmad, A. Hagfeldt, S.G. Hashmi, Advanced research trends in dye-sensitized solar cells, J. Mater. Chem. A. 9 (2021) 10527–10545. https://doi.org/10.1039/D1TA00690H.

[8] M. Stojanović, N. Flores-Diaz, Y. Ren, N. Vlachopoulos, L. Pfeifer, Z. Shen, Y. Liu, S.M. Zakeeruddin, J.V. Milić, A. Hagfeldt, The Rise of Dye-Sensitized Solar Cells: From Molecular Photovoltaics to Emerging Solid-State Photovoltaic Technologies, Helv. Chim. Acta. 104 (2021) e2000230.

[9] N. Vlachopoulos, A. Hagfeldt, I. Benesperi, M. Freitag, G. Hashmi, G. Jia, R.A. Wahyuono, J. Plentz, B. Dietzek, New approaches in component design for dye-sensitized solar cells, Sustain. Energy Fuels. 5 (2021) 367–383.

[10] A.B. Muñoz-García, I. Benesperi, G. Boschloo, J.J. Concepcion, J.H. Delcamp, E.A. Gibson, G.J. Meyer, M. Pavone, H. Pettersson, A. Hagfeldt, M. Freitag, Dye-sensitized solar cells strike back, Chem. Soc. Rev. 50 (2021) 12450–12550. https://doi.org/10.1039/D0CS01336F.

[11] M. Aftabuzzaman, S. Sarker, C. Lu, H.K. Kim, In-depth understanding of the energy loss and efficiency limit of dye-sensitized solar cells under outdoor and indoor conditions, J. Mater. Chem. A. 9 (2021) 24830–24848. https://doi.org/10.1039/D1TA03309C.

[12] K.M. Kim, H.K. Kim, Highly efficient gel electrolytes by end group modified PEG-based ABA triblock copolymers for quasi-solid-state dye-sensitized solar cells, Chem. Eng. J. 420 (2021) 129899.

[13] D. Zhang, M. Stojanovic, Y. Ren, Y. Cao, F.T. Eickemeyer, E. Socie, N. Vlachopoulos, J.-E. Moser, S.M. Zakeeruddin, A. Hagfeldt, A molecular photosensitizer achieves a V oc of 1.24 V enabling highly efficient and stable dye-sensitized solar cells with copper (II/I)-based electrolyte, Nat. Commun. 12 (2021) 1–10.

[14] J.V. Vaghasiya, K.K. Sonigara, L. Suresh, M. Panahandeh-Fard, S.S. Soni, S.C. Tan, Efficient power generating devices utilizing low intensity indoor lights via non-radiative energy transfer mechanism from organic ionic redox couples, Nano Energy. 60 (2019) 457–466.

[15] P.K. Enaganti, S. Soman, S.S. Devan, S.C. Pradhan, A.K. Srivastava, J.M. Pearce, S. Goel, Dye-sensitized solar cells as promising candidates for underwater photovoltaic applications, Prog. Photovolt. Res. Appl. (2022) 1-8. https://doi.org/10.1002/pip.3535.

[16] J. Wu, Z. Lan, J. Lin, M. Huang, Y. Huang, L. Fan, G. Luo, Electrolytes in Dye-Sensitized Solar Cells, Chem. Rev. 115 (2015) 2136–2173. https://doi.org/10.1021/cr400675m.

[17] M. Masud, K.M. Kim, H.K. Kim, Polymer gel electrolytes based on PEG-functionalized ABA triblock copolymers for quasi-solid-state dye-sensitized solar cells: Molecular engineering and key factors, ACS Appl Mater Interfaces. 12 (2020) 42067–42080.

[18] K.M. Kim, Masud, J.-M. Ji, H.K. Kim, PAN-Based Triblock Copolymers Tailor-Made by Reversible Addition–Fragmentation Chain Transfer Polymerization for High-Performance Quasi-Solid State Dye-Sensitized Solar Cells, ACS Appl. Energy Mater. 4 (2020) 1302–1312.

[19] C.-Y. Chen, M. Wang, J.-Y. Li, N. Pootrakulchote, L. Alibabaei, C. Ngoc-le, J.-D. Decoppet, J.-H. Tsai, C. Grätzel, C.-G. Wu, others, Highly efficient light-harvesting ruthenium sensitizer for thin-film dye-sensitized solar cells, ACS Nano. 3 (2009) 3103–3109.

[20] X. He, Y. Guo, X. Li, J. Liu, In situ ligand-free growth of TiO2-escapsulated Au nanocomposites on photoanode for efficient dye sensitized solar cells, Chem. Eng. J. 396 (2020) 125302.

[21] B. Pang, M. Zhang, C. Zhou, H. Dong, S. Ma, J. Feng, Y. Chen, L. Yu, L. Dong, Heterogeneous FeNi3/NiFe2O4 nanoparticles with modified graphene as electrocatalysts for high performance dye-sensitized solar cells, Chem. Eng. J. 405 (2021) 126944.

[22] S. Mathew, A. Yella, P. Gao, R. Humphry-Baker, B.F. Curchod, N. Ashari-Astani, I. Tavernelli, U. Rothlisberger, M.K. Nazeeruddin, M. Grätzel, Dye-sensitized solar cells with 13% efficiency achieved through the molecular engineering of porphyrin sensitizers, Nat. Chem. 6 (2014) 242–247.

[23] A. Yella, H.-W. Lee, H.N. Tsao, C. Yi, A.K. Chandiran, M.K. Nazeeruddin, E.W.-G. Diau, C.-Y. Yeh, S.M. Zakeeruddin, M. Gratzel, Porphyrin-Sensitized Solar Cells with Cobalt (II/III)-Based Redox Electrolyte Exceed 12 Percent Efficiency, Science. 334 (2011) 629–634. https://doi.org/10.1126/science.1209688.

[24] C.-C. Chen, J.-S. Chen, V.S. Nguyen, T.-C. Wei, C.-Y. Yeh, Double Fence Porphyrins that are Compatible with Cobalt (II/III) Electrolyte for High-Efficiency Dye-Sensitized Solar Cells, Angew. Chem. Int. Ed. 60 (2021) 4886–4893.

[25] K. Kakiage, Y. Aoyama, T. Yano, K. Oya, J. Fujisawa, M. Hanaya, Highly-efficient dye-sensitized solar cells with collaborative sensitization by silyl-anchor and carboxy-anchor dyes, Chem. Commun. 51 (2015) 15894–15897.

[26] J.-M. Ji, H. Zhou, Y.K. Eom, C.H. Kim, H.K. Kim, 14.2% Efficiency Dye-Sensitized Solar Cells by Co-sensitizing Novel Thieno [3, 2-b] indole-Based Organic Dyes with a Promising Porphyrin Sensitizer, Adv. Energy Mater. 10 (2020) 2000124.

[27] N. Jiang, T. Sumitomo, T. Lee, A. Pellaroque, O. Bellon, D. Milliken, H. Desilvestro, High temperature stability of dye solar cells, Sol. Energy Mater. Sol. Cells. 119 (2013) 36–50.

[28] B. O'Regan, F. Lenzmann, R. Muis, J. Wienke, A solid-state dye-sensitized solar cell fabricated with pressure-treated P25-TiO2 and CuSCN: analysis of pore filling and IV characteristics, Chem. Mater. 14 (2002) 5023–5029.

[29] A. Hagfeldt, G. Boschloo, L. Sun, L. Kloo, H. Pettersson, Dye-sensitized solar cells, Chem. Rev. 110 (2010) 6595–6663.

[30] B. Lee, J. He, R.P. Chang, M.G. Kanatzidis, All-solid-state dye-sensitized solar cells with high efficiency, Nature. 485 (2012) 486–489.

[31] F. Fabregat-Santiago, J. Bisquert, L. Cevey, P. Chen, M. Wang, S.M. Zakeeruddin, M. Grätzel, Electron transport and recombination in solid-state dye solar cell with spiro-OMeTAD as hole conductor, J. Am. Chem. Soc. 131 (2008) 558–562.

[32] W. Zhang, R. Zhu, F. Li, Q. Wang, B. Liu, High-performance solid-state organic dye sensitized solar cells with P3HT as hole transporter, J. Phys. Chem. C. 115 (2011) 7038–7043.

[33] Y. Cao, Y. Saygili, A. Ummadisingu, J. Teuscher, J. Luo, N. Pellet, F. Giordano, S.M. Zakeeruddin, J.-E. Moser, M. Freitag, 11% efficiency solid-state dye-sensitized solar cells with copper (II/I) hole transport materials, Nat. Commun. 8 (2017) 1–8.

[34] G. Bousrez, O. Renier, B. Adranno, V. Smetana, A.-V. Mudring, Ionic Liquid-Based Dye-Sensitized Solar Cells—Insights into Electrolyte and Redox Mediator Design, ACS Sustain. Chem. Eng. 9 (2021) 8107–8114. https://doi.org/10.1021/acssuschemeng.1c01057.

[35] P. Ma, Y. Fang, A. Li, B. Wen, H. Cheng, X. Zhou, Y. Shi, H.Y. Yang, Y. Lin, Highly efficient and stable ionic liquid-based gel electrolytes, Nanoscale. 13 (2021) 7140–7151.

[36] M. Thomas, S. Rajiv, Grafted PEO polymeric ionic liquid nanocomposite electrospun membrane for efficient and stable dye sensitized solar cell, Electrochimica Acta. 341 (2020) 136040.

[37] F.-S. Lin, M. Sakthivel, M.-S. Fan, J.-J. Lin, R.-J. Jeng, K.-C. Ho, A novel multifunctional polymer ionic liquid as an additive in iodide electrolyte combined with silver mirror coating counter electrodes for quasi-solid-state dye-sensitized solar cells, J. Mater. Chem. A. 9 (2021) 4907–4921.

[38] C.-P. Lee, K.-C. Ho, Poly (ionic liquid) s for dye-sensitized solar cells: a mini-review, Eur. Polym. J. 108 (2018) 420–428.

[39] S.-K. Tseng, R.-H. Wang, J.-L. Wu, J.P. Jyothibasu, T.-L. Wang, C.-Y. Chu, R.-H. Lee, Synthesis of a series of novel imidazolium-containing ionic liquid copolymers for dye-sensitized solar cells, Polymer. 210 (2020) 123074.

[40] N. Jeon, S.-G. Jo, S.-H. Kim, M.-S. Park, D.-W. Kim, Quasi-solid-state polymer electrolytes based on a polymeric ionic liquid with high ionic conductivity and enhanced stability, J. Electrochem. Sci. Technol. 8 (2017) 257–264.

[41] H.-W. Pang, H.-F. Yu, Y.-J. Huang, C.-T. Li, K.-C. Ho, Electrospun membranes of imidazole-grafted PVDF-HFP polymeric ionic liquids for highly efficient quasi-solid-state dye-sensitized solar cells, J. Mater. Chem. A. 6 (2018) 14215–14223.

[42] M. Thomas, S. Rajiv, Porous membrane of polyindole and polymeric ionic liquid incorporated PMMA for efficient quasi-solid state dye sensitized solar cell, J. Photochem. Photobiol. Chem. 394 (2020) 112464.

[43] W.S. Chi, J.K. Koh, S.H. Ahn, J.-S. Shin, H. Ahn, D.Y. Ryu, J.H. Kim, Highly efficient I2-free solid-state dye-sensitized solar cells fabricated with polymerized ionic liquid and graft copolymer-directed mesoporous film, Electrochem. Commun. 13 (2011) 1349–1352.

[44] W.S. Chi, D.K. Roh, C.S. Lee, J.H. Kim, A shape-and morphology-controlled metal organic framework template for high-efficiency solid-state dye-sensitized solar cells, J. Mater. Chem. A. 3 (2015) 21599–21608.

[45] G. Wang, C. Yan, J. Zhang, S. Hou, W. Zhang, Highly efficient solid-state dye-sensitized solar cells based on hexylimidazolium iodide ionic polymer electrolyte prepared by in situ low-temperature polymerization, J. Power Sources. 345 (2017) 131–136.

[46] A.K. Bharwal, L. Manceriu, C. Iojoiu, J. Dewalque, T. Toupance, L. Hirsch, C. Henrist, F. Alloin, Ionic-Liquid-like Polysiloxane Electrolytes for Highly Stable Solid-State Dye-Sensitized Solar Cells, ACS Appl. Energy Mater. 1 (2018) 4106–4114. https://doi.org/10.1021/acsaem.8b00769.

[47] M.P. Cipolla, G.L. De Gregorio, R. Grisorio, R. Giannuzzi, G. Gigli, G.P. Suranna, M. Manca, An ion conductive polysiloxane as effective gel electrolyte for long stable dye solar cells, J. Power Sources. 356 (2017) 191–199.

[48] H. Pujiarti, H. Bahar, R. Hidayat, Poly (ionic-liquid) from imidazoline-functionalized siloxane prepared by simple sol-gel route for efficient quasi-solid-state DSSC, Mater. Res. Express. 6 (2019) 075507.

[49] M. Čolović, J. Volavšek, E. Stathatos, N.Č. Korošin, M. Šobak, I. Jerman, Amphiphilic POSS-based ionic liquid electrolyte additives as a boost for dye-sensitized solar cell performance, Sol. Energy. 183 (2019) 619–631.

[50] A.K. Bharwal, L. Manceriu, F. Alloin, C. Iojoiu, J. Dewalque, T. Toupance, C. Henrist, Tuning bimodal porosity in TiO2 photoanodes towards efficient solid-state dye-sensitized solar cells comprising polysiloxane-based polymer electrolyte, Microporous Mesoporous Mater. 273 (2019) 226–234.

[51] A.K. Bharwal, L. Manceriu, F. Alloin, C. Iojoiu, J. Dewalque, T. Toupance, C. Henrist, Bimodal titanium oxide photoelectrodes with tuned porosity for improved light harvesting and polysiloxane-based polymer electrolyte infiltration, Sol. Energy. 178 (2019) 98–107.

[52] Y. Rong, X. Li, G. Liu, H. Wang, Z. Ku, M. Xu, L. Liu, M. Hu, Y. Yang, M. Zhang, Monolithic quasi-solid-state dye-sensitized solar cells based on iodine-free polymer gel electrolyte, J. Power Sources. 235 (2013) 243–250.

[53] J.-L. Lan, T.-C. Wei, S.-P. Feng, C.-C. Wan, G. Cao, Effects of iodine content in the electrolyte on the charge transfer and power conversion efficiency of dye-sensitized solar cells under low light intensities, J. Phys. Chem. C. 116 (2012) 25727–25733.

[54] B. Mohamad Ali, K. Ashok Kumar, I. Bargathulla, S. Sathiyaraj, A. Sultan Nasar, Elimination of 50% Iodine and Excellent Performance of Dye-Sensitized Solar Cell Enabled by TEMPO Radical Dendrimer–Iodide Dual Redox Systems, ACS Appl. Energy Mater. 3 (2020) 10506–10514.

[55] H. Wang, H. Li, B. Xue, Z. Wang, Q. Meng, L. Chen, Solid-state composite electrolyte LiI/3-hydroxypropionitrile/SiO2 for dye-sensitized solar cells, J. Am. Chem. Soc. 127 (2005) 6394–6401.

[56] W.-C. Yu, L.-Y. Lin, W.-C. Chang, S.-H. Zhong, C.-C. Su, Iodine-free nanocomposite gel electrolytes for quasi-solid-state dye-sensitized solar cells, J. Power Sources. 403 (2018) 157–166.

[57] S.H. Ahn, W.S. Chi, J.T. Park, J.K. Koh, D.K. Roh, J.H. Kim, Direct Assembly of Preformed Nanoparticles and Graft Copolymer for the Fabrication of Micrometer-thick, Organized TiO2 Films: High Efficiency Solid-state Dye-sensitized Solar Cells, Adv. Mater. 24 (2012) 519–522.

[58] S.H. Ahn, W.S. Chi, D.J. Kim, S.Y. Heo, J.H. Kim, Honeycomb-Like Organized TiO2 Photoanodes with Dual Pores for Solid-State Dye-Sensitized Solar Cells, Adv. Funct. Mater. 23 (2013) 3901–3908.

[59] S.H. Ahn, D.J. Kim, W.S. Chi, J.H. Kim, Hierarchical Double-Shell Nanostructures of TiO2 Nanosheets on SnO2 Hollow Spheres for High-Efficiency, Solid-State, Dye-Sensitized Solar Cells, Adv. Funct. Mater. 24 (2014) 5037–5044.

[60] D.K. Roh, W.S. Chi, H. Jeon, S.J. Kim, J.H. Kim, High efficiency solid-state dye-sensitized solar cells assembled with hierarchical anatase pine tree-like TiO2 nanotubes, Adv. Funct. Mater. 24 (2014) 379–386.

[61] R.R. Lunt, V. Bulovic, Transparent, near-infrared organic photovoltaic solar cells for window and energy-scavenging applications, Appl. Phys. Lett. 98 (2011) 61.

[62] R. Alkarsifi, Y.A. Avalos-Quiroz, P. Perkhun, X. Liu, M. Fahlman, A.K. Bharwal, C.M. Ruiz, D. Duché, J.-J. Simon, C. Videlot-Ackermann, Organic–inorganic doped nickel oxide nanocrystals for hole transport layers in inverted polymer solar cells with color tuning, Mater. Chem. Front. 5 (2021) 418–429.

[63] G.P. Kini, S.J. Jeon, D.K. Moon, Latest Progress on Photoabsorbent Materials for Multifunctional Semitransparent Organic Solar Cells, Adv. Funct. Mater. 31 (2021) 2007931.

[64] H. Wang, J. Li, H.A. Dewi, N. Mathews, S. Mhaisalkar, A. Bruno, Colorful Perovskite Solar Cells: Progress, Strategies, and Potentials, J. Phys. Chem. Lett. 12 (2021) 1321–1329.

[65] Y. Ren, Y. Cao, D. Zhang, S.M. Zakeeruddin, A. Hagfeldt, P. Wang, M. Grätzel, A blue photosensitizer realizing efficient and stable green solar cells via color tuning by the electrolyte, Adv. Mater. 32 (2020) 2000193.

[66] Y. Yang, C. Liu, H. Kanda, Y. Ding, H. Huang, H. Chen, B. Ding, Y. Liang, X. Liu, M. Cai, Expanded Phase Distribution in Low Average Layer-Number 2D Perovskite Films: Toward Efficient Semitransparent Solar Cells, Adv. Funct. Mater. (n.d.) 2104868.

[67] A. Roy, A. Ghosh, S. Bhandari, P. Selvaraj, S. Sundaram, T.K. Mallick, Color comfort evaluation of dye-sensitized solar cell (DSSC) based building-integrated photovoltaic (BIPV) glazing after 2 years of ambient exposure, J. Phys. Chem. C. 123 (2019) 23834–23837.

[68] Q. Huaulmé, V.M. Mwalukuku, D. Joly, J. Liotier, Y. Kervella, P. Maldivi, S. Narbey, F. Oswald, A.J. Riquelme, J.A. Anta, Photochromic dye-sensitized solar cells with light-driven adjustable optical transmission and power conversion efficiency, Nat. Energy. 5 (2020) 468–477.

[69] W. Naim, V. Novelli, I. Nikolinakos, N. Barbero, I. Dzeba, F. Grifoni, Y. Ren, T. Alnasser, A. Velardo, R. Borrelli, Transparent and Colorless Dye-Sensitized Solar Cells Exceeding 75% Average Visible Transmittance, JACS Au. 1 (2021) 409–426.

[70] F. Grifoni, M. Bonomo, W. Naim, N. Barbero, T. Alnasser, I. Dzeba, M. Giordano, A. Tsaturyan, M. Urbani, T. Torres, Toward Sustainable, Colorless, and Transparent Photovoltaics: State of the Art and Perspectives for the Development of Selective Near-Infrared Dye-Sensitized Solar Cells, Adv. Energy Mater. (2021) 2101598.

[71] D.A. Chalkias, C. Charalampopoulos, A.K. Andreopoulou, A. Karavioti, E. Stathatos, Spectral engineering of semi-transparent dye-sensitized solar cells using new triphenylamine-based dyes and an iodine-free electrolyte for greenhouse-oriented applications, J. Power Sources. 496 (2021) 229842.

[72] A.K. Bharwal, G.D. Salian, L. Manceriu, A. Mahmoud, F. Alloin, C. Iojoiu, T. Djenizian, C.M. Ruiz, M. Pasquinelli, T. Toupance, C. Olivier, D. Duché, J.-J. Simon, C. Henrist, Plasticized I2-free polysiloxane ionic conductors as electrolytes for stable and flexible solid-state dye-sensitized solar cells, Appl. Surf. Sci. Adv. 5 (2021) 100120. https://doi.org/10.1016/j.apsadv.2021.100120.

[73] S.-J. Seo, K.A. Bialecka, M.-S. Kang, A. Hinsch, S.-H. Moon, In-situ analyses of triiodide formation in an iodine-free electrolyte for dye-sensitized solar cells using electro-diffuse-reflection spectroscopy (EDRS), J. Power Sources. 275 (2015) 675–680.

[74] C. Prehal, H. Fitzek, G. Kothleitner, V. Presser, B. Gollas, S.A. Freunberger, Q. Abbas, Persistent and reversible solid iodine electrodeposition in nanoporous carbons, Nat. Commun. 11 (2020) 1–10.

[75] A.K. Bharwal, N.A. Nguyen, C. Iojoiu, C. Henrist, F. Alloin, New polysiloxane bearing imidazolium iodide side chain as electrolyte for photoelectrochemical cell, Solid State Ion. 307 (2017) 6–13. https://doi.org/10.1016/j.ssi.2017.05.004.

[76] Solar Spectra, (n.d.). https://www.nrel.gov/grid/solar-resource/spectra.html (accessed April 11, 2022).

[77] B. Garcia, S. Lavallée, G. Perron, C. Michot, M. Armand, Room temperature molten salts as lithium battery electrolyte, Electrochimica Acta. 49 (2004) 4583–4588.

[78] H.-D. Nguyen, G.-T. Kim, J. Shi, E. Paillard, P. Judeinstein, S. Lyonnard, D. Bresser, C. Iojoiu, Nanostructured multi-block copolymer single-ion conductors for safer high-performance lithium batteries, Energy Environ. Sci. 11 (2018) 3298–3309.

[79] C. Wang, X. Li, J. Zhou, W. Tian, J. Ji, Y. Wu, S. Tan, Poly (ionic liquid) Bridge Joining Smectic Lamellar Conducting Channels in Photoelectrochemical Devices as High-Performance Solid-State Electrolytes, ACS Appl. Energy Mater. 4 (2021) 9479–9486.

[80] Y. Rong, Z. Ku, M. Xu, L. Liu, M. Hu, Y. Yang, J. Chen, A. Mei, T. Liu, H. Han, Efficient monolithic quasi-solid-state dye-sensitized solar cells based on poly (ionic liquids) and carbon counter electrodes, RSC Adv. 4 (2014) 9271–9274.

[81] A. Zaban, M. Greenshtein, J. Bisquert, Determination of the electron lifetime in nanocrystalline dye solar cells by open-circuit voltage decay measurements, ChemPhysChem. 4 (2003) 859–864.

[82] P. Perkhun, W. Köntges, F. Pourcin, D. Esteoulle, E. Barulina, N. Yoshimoto, P. Pierron, O. Margeat, C. Videlot-Ackermann, A.K. Bharwal, High-Efficiency Digital Inkjet-Printed Non-Fullerene Polymer Blends Using Non-Halogenated Solvents, Adv. Energy Sustain. Res. 2 (2021) 2000086.

[83] M. Mohammadnezhad, G.S. Selopal, O. Cavuslar, D. Barba, E.G. Durmusoglu, H.Y. Acar, Z.M. Wang, G.P. Lopinski, B. Stansfield, H. Zhao, Gold nanoparticle decorated carbon nanotube nanocomposite for dye-sensitized solar cell performance and stability enhancement, Chem. Eng. J. 421 (2021) 127756.

[84] M. Mohammadnezhad, G.S. Selopal, Z.M. Wang, B. Stansfield, H. Zhao, F. Rosei, Role of carbon nanotubes to enhance the long-term stability of dye-Sensitized solar cells, ACS Photonics. 7 (2020) 653–664.

[85] C. Wu, Y. Gong, S. Han, T. Jin, B. Chi, J. Pu, L. Jian, Electrochemical characterization of a novel iodine-free electrolyte for dye-sensitized solar cell, Electrochimica Acta. 71 (2012) 33–38.

[86] I. Jerman, V. Jovanovski, A.Š. Vuk, S.B. Hočevar, M. Gaberšček, A. Jesih, B. Orel, Ionic conductivity, infrared and Raman spectroscopic studies of 1-methyl-3-propylimidazolium iodide ionic liquid with added iodine, Electrochimica Acta. 53 (2008) 2281–2288.

[87] E. Tanaka, N. Robertson, Polyiodide solid-state dye-sensitized solar cell produced from a standard liquid I-/I 3- electrolyte, J. Mater. Chem. A. 8 (2020) 19991–19999.

[88] Z. Mao, Y. Ye, H. Lv, X.X. Han, Y. Park, L. Zang, B. Zhao, Y.M. Jung, Direct Dynamic Evidence of Charge Separation in a Dye-Sensitized Solar Cell Obtained under

Operando Conditions by Raman Spectroscopy, Angew. Chem. 132 (2020) 10872–10876.

[89] W. Kubo, K. Murakoshi, T. Kitamura, S. Yoshida, M. Haruki, K. Hanabusa, H. Shirai, Y. Wada, S. Yanagida, Quasi-solid-state dye-sensitized TiO2 solar cells: effective charge transport in mesoporous space filled with gel electrolytes containing iodide and iodine, J. Phys. Chem. B. 105 (2001) 12809–12815.

[90] N. Papageorgiou, M. Grätzel, P.P. Infelta, On the relevance of mass transport in thin layer nanocrystalline photoelectrochemical solar cells, Sol. Energy Mater. Sol. Cells. 44 (1996) 405–438.

[91] S. Rafique, I. Rashid, R. Sharif, Cost effective dye sensitized solar cell based on novel Cu polypyrrole multiwall carbon nanotubes nanocomposites counter electrode, Sci. Rep. 11 (2021) 1–8.

[92] Q. Wang, J.-E. Moser, M. Grätzel, Electrochemical impedance spectroscopic analysis of dye-sensitized solar cells, J. Phys. Chem. B. 109 (2005) 14945–14953.

[93] Z. Yu, S. You, C. Wang, C. Bu, S. Bai, Z. Zhou, Q. Tai, W. Liu, S. Guo, X. Zhao, Efficient dye-sensitized solar cells employing highly environmentally-friendly ubiquinone 10 based I 2-free electrolyte inspired by photosynthesis, J. Mater. Chem. A. 2 (2014) 9007–9010.

[94] J. Xia, N. Masaki, M. Lira-Cantu, Y. Kim, K. Jiang, S. Yanagida, Influence of doped anions on poly (3, 4-ethylenedioxythiophene) as hole conductors for iodine-free solid-state dye-sensitized solar cells, J. Am. Chem. Soc. 130 (2008) 1258–1263.

[95] C.-M. Lan, S.-E. Liu, J.-W. Shiu, J.-Y. Hu, M.-H. Lin, E.W.-G. Diau, Formation of size-tunable dandelion-like hierarchical rutile titania nanospheres for dye-sensitized solar cells, Rsc Adv. 3 (2013) 559–565.

[96] M.N. Mustafa, Y. Sulaiman, Review on the effect of compact layers and light scattering layers on the enhancement of dye-sensitized solar cells, Sol. Energy. 215 (2021) 26–43.

[97] S.-W. Lee, K.-S. Ahn, K. Zhu, N.R. Neale, A.J. Frank, Effects of TiCl4 treatment of nanoporous TiO2 films on morphology, light harvesting, and charge-carrier dynamics in dye-sensitized solar cells, J. Phys. Chem. C. 116 (2012) 21285–21290.

[98] P.M. Sommeling, B.C. O'Regan, R.R. Haswell, H.J.P. Smit, N.J. Bakker, J.J.T. Smits, J.M. Kroon, J.A.M. Van Roosmalen, Influence of a TiCl4 post-treatment on nanocrystalline TiO2 films in dye-sensitized solar cells, J. Phys. Chem. B. 110 (2006) 19191–19197.

[99] J.-H. Park, J.-Y. Kim, J.-H. Kim, C.-J. Choi, H. Kim, Y.-E. Sung, K.-S. Ahn, Enhanced efficiency of dye-sensitized solar cells through TiCl4-treated, nanoporous-layer-covered TiO2 nanotube arrays, J. Power Sources. 196 (2011) 8904–8908.

[100] Z.-S. Wang, H. Kawauchi, T. Kashima, H. Arakawa, Significant influence of TiO2 photoelectrode morphology on the energy conversion efficiency of N719 dye-sensitized solar cell, Coord. Chem. Rev. 248 (2004) 1381–1389.